CITATION

Lentini, C.A.D., J.M. Magalhães, J.C.B. da Silva, and J.A. Lorenzzetti. 2016. Transcritical flow and generation of internal solitary waves off the Amazon River: Synthetic aperture radar observations and interpretation. *Oceanography* 29(4):187–195, https://doi.org/10.5670/oceanog.2016.88.

DOI

https://doi.org/10.5670/oceanog.2016.88

Transcritical Flow and Generation of Internal Solitary Waves off the Amazon River

Synthetic Aperture Radar Observations and Interpretation

By Carlos A.D. Lentini,
Jorge M. Magalhães,
José C.B. da Silva, and
João A. Lorenzzetti

ABSTRACT. A satellite synthetic aperture radar (SAR) data set facilitates investigation of the two-dimensional structure of internal solitary waves (ISWs) that propagate near the Amazon River mouth. Three distinct groups of waves are identified according to their propagation direction. While cross-shelf ISW propagation has been previously documented, it is found that the majority of the waves propagate along the shelf and upstream of the North Brazilian Current (NBC). These ISWs appear in packets with interpacket separations of ~4 km, mean crest lengths of 10 km, and intersoliton separations of ~500 m. They are observed throughout the entire semidiurnal and fortnightly tidal cycles, but their origin appears to result primarily from the steady NBC, modulated by tidal currents, as it flows over shallow bottom topography. A Froude number analysis considering mode-1 nonhydrostatic linear waves propagating upstream of the NBC is found to be consistent with a regime of transcritical generation in the study region.

INTRODUCTION

Diverse and dynamic features that occur on the continental shelf off the mouth of the Amazon River in the southwest tropical Atlantic Ocean (Figure 1a) include the western boundary North Brazilian Current (NBC), strong tidal constituents, and more than 1,000 km of complex bottom bathymetry (Johns et al., 1998; Hübscher et al., 2002). Here, the Amazon River, which supplies approximately one-fifth of the total freshwater discharge into the world ocean, strongly modulates the surrounding stratification (e.g., Muller-Karger et al., 1988). Its considerable riverine plume often extends several hundred kilometers to the northwest of the river's mouth (Lentz, 1995). These various oceanographic elements play an important role in many related fields of research, including studies of the geological and biological systems distributed along the extensive continental shelf (e.g., Almeida et al., 2005; Moura et al., 2016). Although the Amazon shelf has been the subject of numerous oceanographic studies (e.g., Coles et al., 2013), it has not been fully investigated for the presence of internal waves (IWs).

IWs are important to numerous fields of marine research because they are essentially the equivalent of surface waves but propagate along the ocean's interior pycnocline rather than at the surface. Their existence depends only upon stable
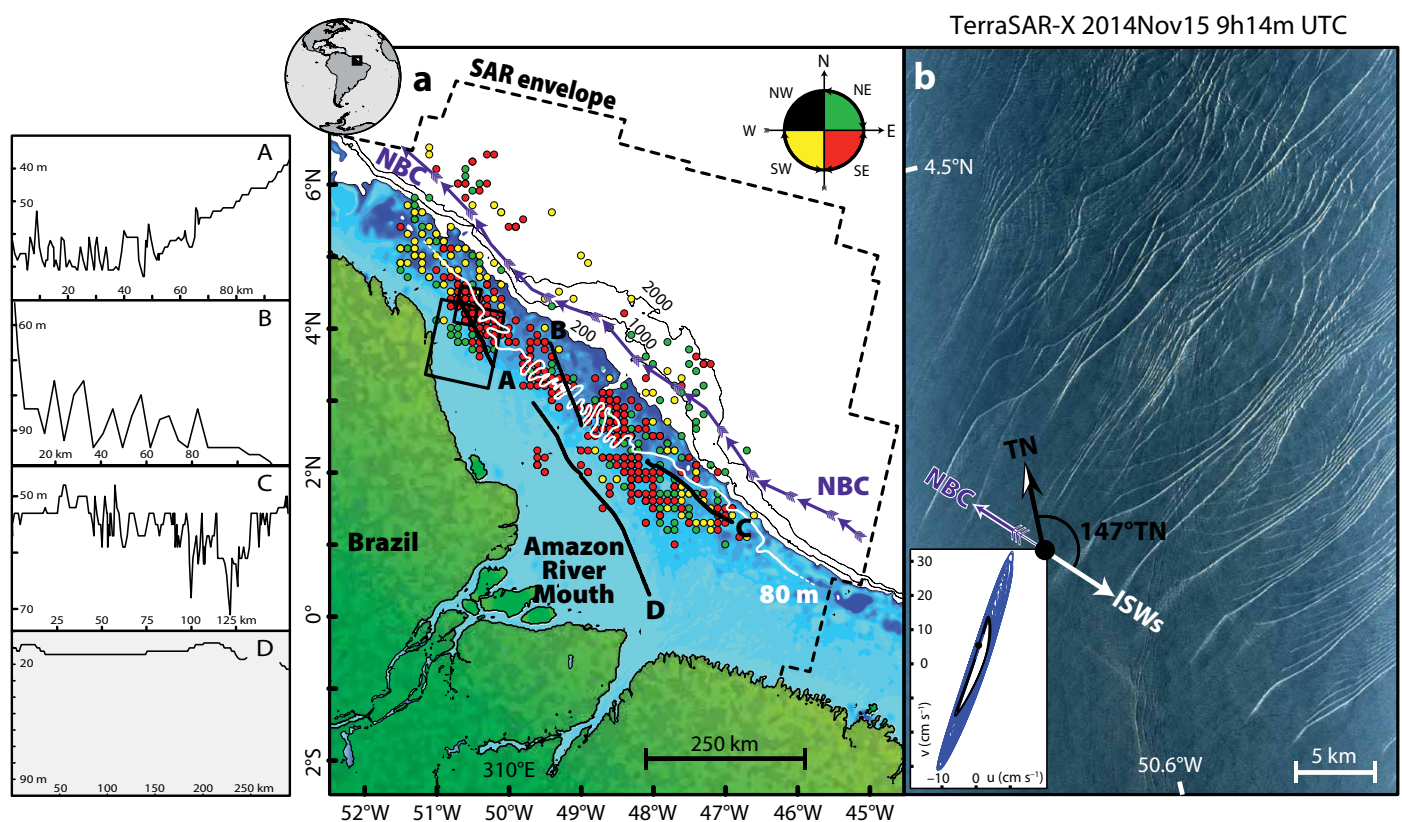
FIGURE 1. (a) Amazon continental shelf and the Amazon River mouth in the southwest Tropical Atlantic (see inset in top-left corner). A synthetic aperture radar (SAR) envelope (black dashed line) encloses an internal solitary wave (ISW) composite map based on 35 images, which are color-coded according to their direction of propagation (see inset in top-right corner). For reference, the continental shelf is shown in blue shading to 200 m with the 80 m isobath highlighted in white. High-resolution bathymetry transects appear as black solid lines, and bottom profiles are shown in panels on the left labeled A to D. Blue arrows indicate the North Brazilian Current (NBC), and the black rectangles depict the SAR acquisitions shown in Figures 1b and 3a. (b) TerraSAR-X acquisition dated November 15, 2014, at 09:14 UTC. Tidal ellipses computed every 10 minutes at approximately 4.2°N and 50.5°W for a period of 20 days (centered at the image's acquisition time) are shown in the bottom-left corner. The black dot in the tidal ellipses represents the image's acquisition time, and the solid black line spans a semidiurnal tidal cycle.

stratification that, together with multiple generation mechanisms, makes them ubiquitous features in the world ocean. Although IWs may arise from many different processes, most are of tidal origin. They form as stratified tidal currents flow over irregular bottom topography and create internal tides (i.e., IWs of tidal frequency) that may propagate for long distances and may steepen and disintegrate into smaller-scale internal solitary waves (ISWs; see Jackson et al., 2012, and references therein; Alford et al., 2015; da Silva et al., 2015).

The generation of ISWs that result from flow over small-scale bottom topography is particularly relevant to the present study. A critical condition is met when the total flow (i.e. tidal + steady currents) matches the internal wave propagation speed (i.e., its phase speed) sustained by local stratification. In other words, when the seafloor has undulating features whose crests are nearly perpendicular to the flow field, nonlinear internal waves can be generated as a result of near-critical flow (see, Jackson et al., 2012, and references therein). In this case, internal wave amplitudes will grow as energy is drawn from the mean flow. This ultimately leads to development of strong isopycnal perturbations near the underwater obstacles, and these perturbations frequently evolve into ISW trains (Melville and Helfrich, 1987; Farmer and Armi, 1999).

ISWs can propagate for several hundreds of kilometers, carrying both mass and momentum (Inall et al., 2001; Shroyer et al., 2010) and thus possibly contributing to remote turbulence, mixing, and sediment resuspension (e.g., Quaresma et al., 2007; Klymak et al., 2012; Lamb, 2014). Shallow water internal wave propagation is particularly favorable for producing strong vertical shear and mixing, including generation of Kelvin-Helmholtz instabilities (see Moum et al., 2003, their Figure 14). Under these conditions, energy dissipates (and is possibly transferred to smaller-scale turbulence) as ISWs propagate over

the shelf. This is especially important along the Amazon River mouth, where substantial amounts of freshwater and bottom sediments are fed into the open ocean. Therefore, ISWs in this region are likely to be important in the local dynamics of the Amazon River mouth and affect features ranging from oil and gas structures (as shown in http://app.anp.gov.br and discussed in Almeida et al., 2005) to reef systems that extend for more than 1,000 km (Moura et al., 2016).

Previous Brazilian coastal work includes studies of the intense semidiurnal ISW activity off Rio de Janeiro (Lorenzzetti and Dias, 2013). Strong semidiurnal waves have also been documented off the Amazon shelf, where large-scale ISWs in the southwest tropical Atlantic propagate offshore in a general northeast direction (Ivanov et al., 1990; Brandt et al., 2002; Jackson, 2007; Magalhaes et al., 2016). Finally, a collection of synthetic aperture radar (SAR) images acquired off the Amazon River mouth reveals cross-shelf ISW activity approximately between April and October (Jackson, 2004). According to SAR data collected by Jackson (2004), interpacket separations were found to be between roughly 30 km and 45 km (indicating a tidal origin), while individual soliton separations were found to be between 250 m and 500 m.

Despite these previous studies, a model of the full two-dimensional horizontal structure of the ISWs that propagate along the Amazon continental shelf has still not been fully developed to define its spatial characteristics, seasonal distribution, and possible generation mechanisms. The present study is motivated by an extended SAR data set acquired across the Amazon River mouth that reveals for the first time the presence of high-frequency ISW packets propagating upstream of the NBC.

In this article, we first provide the study region's oceanographic background. We then discuss the SAR data set and analyze results concerning the ISW dynamics, emphasizing details of the generation

of mode-1 ISWs propagating upstream of the NBC and over variable bottom topography. The final section of the paper summarizes our study and presents some concluding remarks.

STUDY REGION

Stretching for more than 1,000 km, the Amazon continental shelf (blue shading in Figure 1a) is one of the most pristine environments in the southwest tropical Atlantic (Moura et al., 2016). It is approximately 300 km wide near the Amazon River mouth and narrows to little more than 100 km to the northwest and southeast. A broad inner shelf with waters shallower than 30 m extends from the coast approximately 100 km toward the open ocean (Castro and Miranda, 1998). A narrower mid-shelf region then follows, with depths up to 60 m, which in turn descends toward the open ocean to an outer shelf of nearly uniform width (defined here in the same fashion as in Johns et al., 1998). The shelf exhibits rough seafloor topography, especially around the 80 m isobath between 47°W and 51°W and 1°N and 4°N (see left panels A–D in Figure 1 and Hübscher et al., 2002), along with complex hydrodynamics resulting from the Amazon River plume, strong trade winds, semidiurnal tides, and NBC variability—all of which are closely related to ISW dynamics.

The Amazon River outflow is seasonally variable, increasing between May and July, and decreasing between October and November (Coe et al., 2002). Its large plume, often identified as a well-defined haline front extending preferentially to the northwest, contains nutrients, suspended sediments, and dissolved material. Simulations by Nikiema et al. (2007) reveal the plume's extent to be governed mainly by the NBC and the trade winds. Note that the Intertropical Convergence Zone in the study region exhibits north-south seasonal variability, resulting in stronger winds between January and April and weaker winds between July and October (Castro and Miranda, 1998).

The Amazon plume's salinity front is

also modulated by powerful tidal currents, which are mostly oriented in the cross-shelf direction (see inset in Figure 1b, and also Figure 5 in Geyer et al., 1996). The mainly semidiurnal barotropic tide intensifies north of 1.5°N, with amplitudes as high as 3 m and strong currents up to 2.0 m s^{-1} (Beardsley et al., 1995). Therefore, a strong tidal contribution to ISW generation is anticipated, which would create mainly cross-shelf propagating internal waves (as those pre-

variability showing maxima between July and August and minima between April and May—but that are mainly restricted to the region beyond the outer shelf. Additional current meters in the mid and outer shelf moored just southeast of the SAR image shown in Figure 1b indicate that weak topographic steering allows some NBC flow variability to extend into shallower waters, which at depths of ~100 m is approximately 20 cm s^{-1} (see Tables 1a and 1b in Johns et al., 1998).

> " The present study provides convincing evidence of transcritical flow along the shelf and is consistent with theories of internal wave resonant generation, in which the [North Brazilian Current] (modulated by the tides) flows over shallow seafloor topography and is likely to generate upstream-propagating waves. "

sented in Jackson, 2004). However, the SAR image shown in Figure 1b (along with many other images of its kind) reveals a powerful ISW field along the Amazon shelf that instead propagates along the shelf. Surprisingly, tidal currents in the along-shelf direction are weak compared to the across-shelf component, ranging only from 5 cm s^{-1} to 20 cm s^{-1} (see inset in Figure 1b). Hence, generation of the along-shelf propagating waves must involve an additional forcing mechanism. The NBC is a possible candidate, because it is oriented along the continental shelf (see dark blue arrows in Figure 1a) and hence along the main axis of ISW propagation. Based on a series of current meter observations, Johns et al. (1998) describe alongshore currents of the order of 1 m s^{-1} that flow below the plume layer (generally considered deeper than 3 m), with seasonal

SAR ANALYSIS

Satellite SAR images have motivated a significant amount of IW research because of this technique's ability to render the two-dimensional horizontal structure of these waves. SARs are very efficient in exploring areas not yet surveyed in detail for the presence of ISWs. The sea surface roughness generated by ISWs is detectable as surface signatures in SAR images (Alpers, 1985; da Silva et al., 1998).

Figure 1b provides a typical SAR view of the study region, using a blue composite rather than the traditional grayscale. This image was acquired on November 15, 2014, at 09:14 UTC, as TerraSAR-X flew over the Amazon shelf (see Figure 1a for location), covering an area of approximately 30 × 50 km^2. The image reveals the details of a series of intense ISW surface signatures, where brighter strips are followed by darker

ones when compared to the unperturbed ambient backscattering. These signatures are characteristic manifestations of mode-1 ISWs propagating along a stratified pycnocline, where the waves' velocity convergence and divergence patterns increase and decrease the Bragg scattering, resulting in lighter and darker patches, respectively. Further inspection, in the same fashion as Thompson and Gasparovic (1986), indicates multiple wave packets propagating alongshore in waters depths of ~80 m, with a strong southeast component (against the NBC). The average interpacket distances range from 3 km to 5 km. We note that these packets do not have wavelengths typical of long, mode-1 IWs (with semidiurnal periods), which are approximately 30 km for these shallow waters (as those presented in Jackson, 2004).

Motivated by these observations, we assembled a representative data set of 51 SAR images acquired over the study region to investigate the full two-dimensional structure of the ISW field propagating along the Amazon continental shelf. The data set includes 34 RADARSAT acquisitions (28 in extended low mode and six in ScanSAR narrow mode), one ERS-SAR and seven Envisat-ASAR images (four in wide swath mode and three in image precision mode), and nine TerraSAR-X acquisitions (eight in stripmap mode and one in spotlight mode). The data set spans November 1993 to April 2015, during which SAR imagery was collected for all months except July, September, October, and December. We further note that this particular data set, which combines multiple satellite sources and a number of different acquisition modes, enables extensive views across the study region (several hundred kilometers wide) along with detailed spatial resolutions (as high as 1 m in some cases).

Significant ISW activity over the shelf was found in 35 of the initial 51 images, while hardly any along-shelf propagation was observed in waters deeper than 200 m. The ISW observations in Figure 2a include semidiurnal and fortnightly

tidal cycles, avoiding the usual tidal aliasing typical of SAR data sets. Note that, according to da Silva et al. (2015), sun-synchronous polar orbits are phase locked with the fortnightly tidal cycle so that spring-neap tides always correspond approximately to the same semidiurnal tidal phases (i.e., low-high tides).

The composite map in Figure 1a displays all observations according to their direction of propagation. Only the strongest waves identified in each image were included, amounting to a total of 703 packets and 876 individual ISWs. The SAR envelope (dashed black line in Figure 1a) that results from merging all the available observations reveals ISW activity mostly restricted to the mid- and outer shelf between 1°N and 6°N and 52°W and 47°W. The inset in the top right corner shows that the entire data set falls into one of three major categories, divided according to the waves' main directions of propagation. Despite the cross-shelf activity (yellow and green), it is clear that the waves propagating southeastward (red) represent the majority of the observations (as in Figure 1b), while no significant northwestward propagation was found.

Figure 2b plots the ISW propagation direction distribution in this region as observed in the SAR images, confirming the overall view provided by the colored dots in Figure 1a. Recalling the inset in Figure 1b, Figure 2b also suggests a tidal origin is likely for the yellow and green wave observations, as strong cross-shelf components flow across the shelf break (just as in many other coastal regions). Note however that the majority of the ISWs propagate generally against the NBC (as indicated with arrows in Figure 1b). This intriguing set of "red" waves must therefore be related to the steady current (i.e., the NBC), at least to first order, and will be the focus of the remaining investigation. In particular, Figure 2c offers further insight into the horizontal structure of the southeastward-propagating waves, revealing a largely unimodal distribution of crest

lengths that are strongly skewed toward the shorter end. These ISW packets are regularly observed to reach crest lengths ranging up to 15 km, although the majority of observations are characterized by crest lengths around 10 km. Note that, on average, three individual waves were counted per packet in the SAR images. We measured inter-packet distances and wave packet lengths to be approximately 5 km and 1.5 km, respectively.

Finally, Figure 2d presents monthly distributions for the number of SAR acquisitions and the corresponding number of normalized ISW observations propagating in the southeast direction. Despite having no acquisitions for some months, the overall view suggests no significant seasonal variability in the study region.

ISW GENERATION MECHANISM
We now seek a plausible hypothesis for ISW generation, recalling that SAR imagery reveals that the majority of the ISWs are propagating upstream of the

mean flow, if a nominal northwestward direction is assumed for the NBC (see Figure 1). In the shallower mid-shelf, the NBC flow direction means that stratified flow will pass over bottom topography with speeds that are close to the phase velocity of long, linear IWs. These conditions have been shown to be sufficient for generation of upstream-propagating ISWs (e.g., Bogucki et al., 1997; Farmer and Armi, 1999; Cummins et al., 2003).

Figure 3a presents an ERS-1 image from November 27, 1993, acquired at 13:44 UTC, covering an area of approximately 100×110 km^2. This image is unique in that it reveals some important details in the same location as the ISWs seen in Figure 1b. Surface manifestations of seafloor features are observed in the Figure 3a SAR image, mostly oriented northeast-southwest, the same direction as the ISW crests (i.e., perpendicular to the NBC). At the same time, an enlarged section reveals what appear to be the early stages of ISW formation
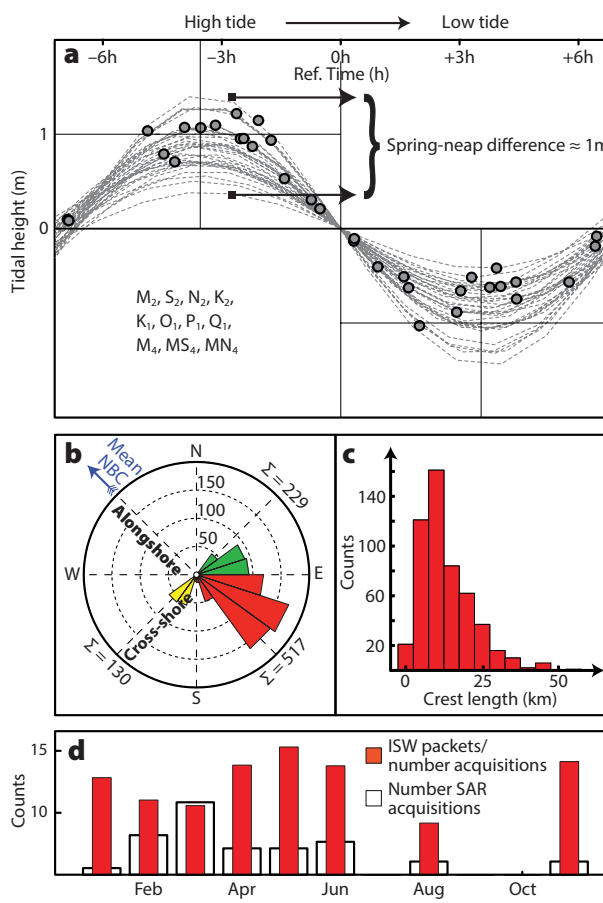
FIGURE 2. (a) Tidal phases for all SAR acquisitions used in the composite map shown in Figure 1a, using the tidal constituents listed in the bottom-left corner. For a meaningful comparison, the time running in the horizontal direction references the transition between high tide and low tide (i.e., when tidal heights change sign), and differences in the vertical range concern different phases of the spring–neap cycle. (b) Propagation direction distribution for all ISWs depicted in Figure 1a. (c) Crest length distribution for the leading ISWs shown in red in panel (b). (d) Monthly distributions for SAR acquisitions used in Figure 1a and normalized number of red ISWs.

on the lee side of some bright features associated with shallow bathymetry (see inset in Figure 3a). We also note that similar SAR bottom features were described in Lodge (1983), and further explained in light of hydrodynamic theory in SAR imagery by Alpers and Hennings (1984) and Shuchman et al. (1985).

Figure 3b compares the seafloor topographic features in Figure 3a and the ISWs in Figure 1b, revealing an approximate match between both SAR manifestations. Note that ISW packets appear to emerge from distinct bottom slopes with approximately the same horizontal scales. These packets are further highlighted in Figure 4 using representative radar transects across the bathymetry and the ISWs (white arrow and thin rectangle in Figure 3b, respectively). Note that radar backscatter transects are usually presented in the literature by means of normalized backscatter intensities (i.e., $(I - I_0)/I_0$, see da Silva et al., 1998), where a reference to a background value (i.e., I_0) is usually averaged over an area away from soliton influence

(see white square in Figure 3b). Figure 4a shows typical length scales in bottom topography to be between approximately 3 km and 5 km and hence in reasonable agreement with interpacket separations shown in Figure 4b.

The data displayed in Figures 3 and 4 are consistent with some generation mechanism resulting from the interaction of the northwestward mean flow (the NBC) and the underlying bottom topography. The forcing effect of bottom topography on stratified flow is usually estimated via an internal or densimetric Froude number, which is used to characterize the corresponding hydraulic state. In essence, the Froude number aims to compare the magnitude of the stratified flow (U) with the corresponding linear IW phase speed (c). In the case of the Amazon shelf, a joint contribution of tides and the NBC needs to be considered as follows:

$$Fr = \frac{U}{c}, \ U = U_{tides} + U_{NBC}. \quad (1)$$

The flow is then said to be in critical ($Fr = 1$), subcritical ($Fr < 1$), or

supercritical ($Fr > 1$) regimes, depending how these two characteristic velocities compare. In practice, a *transcritical regime* is often used to characterize near-critical conditions (Fr of the order of 1), which leads to the generation of upstream-moving trains of solitary waves whose origins are isopycnal disturbances that remain stationary relative to the forcing topography and accumulate energy from the mean flow through resonance. In other words, this means that strong supercritical flows only allow internal perturbations to propagate downstream because the fluid velocity is greater than that of the corresponding linear IW, whereas in subcritical conditions waves will immediately escape upstream of the mean flow (Melville and Helfrich, 1987).

A Froude number analysis is presented in Figure 5, where tidal currents taken across the full length of the Amazon shelf were computed using a regional solution from the Oregon State University Tidal Inversion Software (Egbert and Erofeeva, 2002), which runs at a resolution of 1/60°
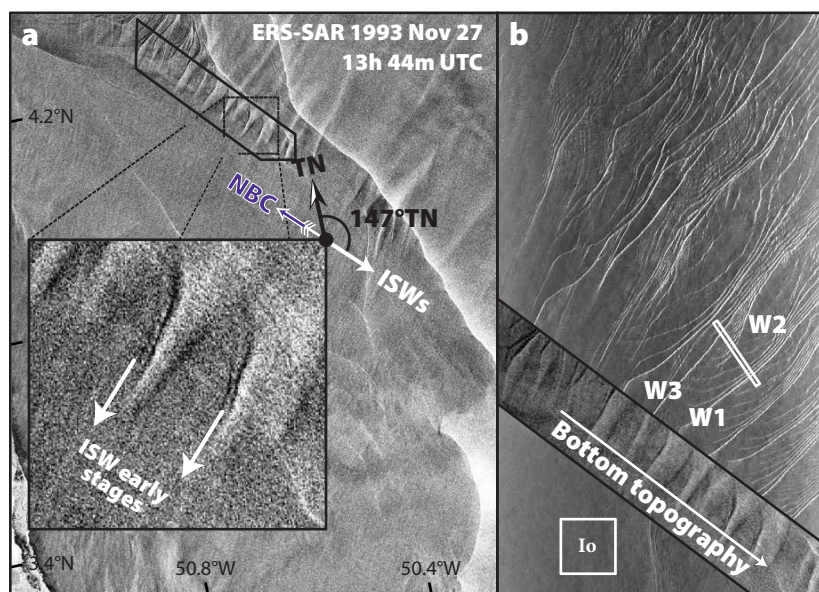
FIGURE 3. (a) ERS-SAR acquisition dated November 27, 1993, at 13:44 UTC. The blue arrow represents a mean NBC flowing toward sea surface manifestations of shallow bottom topography. The inset zooms in on SAR bottom features and highlights high-frequency oscillations, which are interpreted as early stages of ISW formation. (b) Same as Figure 1b, in which the section enclosed by the solid black line in panel (a) has been overlaid to highlight the consistency between the scales and locations of SAR signatures. Transects in Figure 4a,b are depicted by a white arrow and a thin white rectangle, respectively. Three packets labeled W_1 to W_3 are shown together with the unperturbed radar backscatter (i.e., I_0, in the white square).
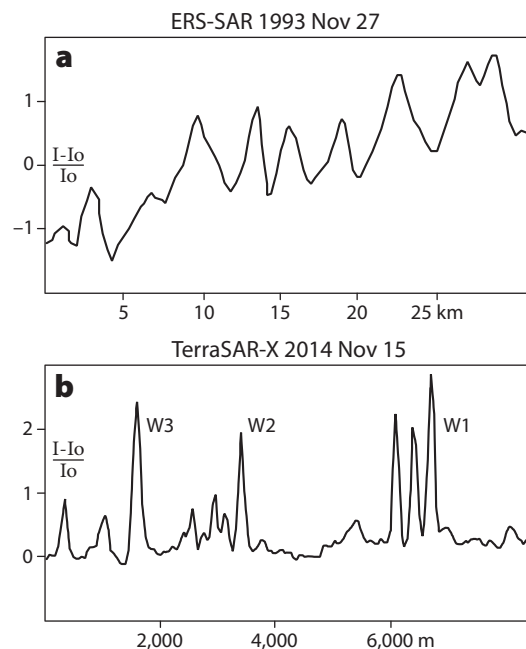
FIGURE 4. (a) Relative intensity radar transect along the white arrow in Figure 3b, showing characteristic scales for the underwater bathymetry to be between approximately 3 km and 5 km. (b) Relative intensity of radar backscatter along the white rectangle in Figure 3b, showing characteristic interpacket and intersoliton separation scales.

and uses all the available tidal constituents (see inset in Figure 1a). We note that no significant spatial variability was found along the shelf where the upstream-propagating waves are observed (red dots in Figure 1a), but the fortnightly cycle shows considerable spring-neap variability—roughly 5 cm s^{-1} to 20 cm s^{-1} in the along ISW propagation direction (147°N on average, see Figure 2b). At the same time, the NBC contribution to the mean flow (i.e., U_{NBC}) was evaluated from Johns et al. (1998, see their Table 1b), who presented moored current meter statistics for a cross-shelf section centered around 3.5°N and 50°W—and thus very close to the ISW observations shown in Figure 1b. Their observational period spans mid-February to mid-April, which includes our period of gathering additional SAR observations (i.e., March), during which they report an essentially vertically sheared flow decreasing linearly with depth over the mid and outer shelf areas (see Figure 5a and their Figure 9). According to these results, a vertical mean flow was estimated as $U_{NBC} = 0.6 \pm 0.1$ m s^{-1} and is used in the Froude number analysis.

A standard boundary value problem was solved in the same fashion as Smyth et al. (2011) and da Silva et al. (2015) to estimate the linear IW phase speed (i.e., c in Equation 1). Appropriate boundary conditions were set considering a rigid lid approximation and a fixed water depth of 80 m for nonhydrostatic waves with an average wavelength of 4 km (estimated from Figure 1b). Local stratification conditions were retrieved from the US National Oceanic and Atmospheric Administration National Ocean Data Center Ocean Climate Laboratory. Figure 5b presents an ensemble of vertical density profiles for March, chosen to represent typical stratification conditions in the study region because they match the period with more SAR observations and are well within the NBC observational period (i.e., from mid-February to mid-April, the period of observations reported in Johns et al., 1998). Intra-monthly

variability in the upper 30 m is quite significant and likely results from the river's plume effect as discussed, for example, in Nikiema et al. (2007). In fact, conditions ranging from near neutral stratification (blue line) to sharp two-layer systems (in green) are found nearly year-round whenever sufficient data are available. Nonetheless, favorable waveguides represent the bulk of the observations (typical in tropical seas), which are represented here by the mean average profile taken over the shelf (in red) in the region where ISWs were found in Figure 1a.

Figure 5c,d presents the overall effect of these environmental constraints on the hydraulic regime, considering a representative SAR image acquired in March. These data are consistent with the shear and stratification plotted in Figure 5a,b (see also online supplemental Figure S1). Note that spatial characteristics of the upstream-propagating ISWs for all SAR

images acquired in this region between January and November remain essentially similar to those in Figure 1b—demonstrating the consistency of the observations. For simplicity, we consider the absolute Fr magnitude in Figure 5c,d, but in this particular case, the mean flow and the ISWs propagate in opposite directions (see Figure 1). We also recall that a transcritical band is reached when Fr is of the order of 1, which means that isopycnal perturbations may remain "trapped" while draining energy from the mean flow—considered here as $Fr = 1 \pm 0.05$ and highlighted in red in Figure 5c,d. According to Figure 5c, these ISWs were observed shortly after near-critical conditions were met, and hence had a lifetime of at least a few hours (see red arrow and solid red circle). Note that as the semidiurnal cycle unfolds and tidal currents align with or against the mean NBC, Fr values oscillate around one as they
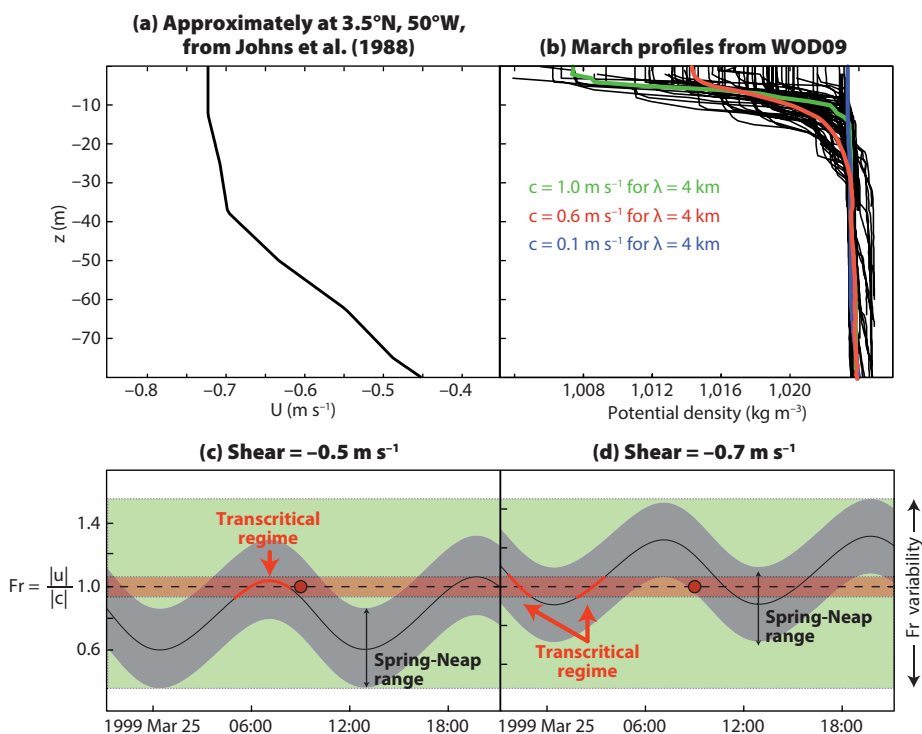
FIGURE 5. (a) Vertical shear along the direction of ISW propagation (i.e., 147°TN) estimated from Johns et al. (1998). (b) Potential density profiles collected within the waves' propagation envelope shown in Figure 1a. Profiles highlighted in green and blue show distinct stratification conditions separated by just two days, and an average profile is shown in red (see text for more details). (c) The solid black line represents internal Froude number estimates according to Equation 1 for approximately two semidiurnal tidal cycles around online supplemental Figure S1 (red circle) and considering a mean vertical shear of 0.5 m s^{-1}. Gray shading represents fortnightly variability of 15 cm s^{-1}. (d) Same as panel (c) considering a mean vertical shear of 0.7 m s^{-1}. The overall variability for both panels is highlighted in green shading.

drift in and out the transcritical band (see solid red sections in the black line). It is also interesting to see that in the particular case of Figure 5c, critical conditions would shift around $Fr = 1$ if an additional variability of 15 cm s^{-1} is considered as part of the fortnightly cycle (seen as the gray shaded area), yielding either more supercritical or more subcritical conditions within just a few days. This introduces a natural source for Fr variability, which competes with that of the mean vertical shear current—set in Figure 5c at 0.5 m s^{-1} (i.e., U_{NBC} = 0.6–0.1 m s^{-1}) and hence at the lower end of the variability envelope presented in Johns et al. (1998). In fact, raising the *shear* variability to 0.7 m s^{-1} shifts the entire plot even further toward the supercritical regime (as shown in Figure 5d). Nonetheless, it is noteworthy that despite this variability, conditions are still consistent with a transcritical regime, regardless of the different conditions assumed for tides and the NBC (see red arrows and solid lines preceding red circles in both panels).

Altogether, the impression from Figure 5 is that there is some variability in the study region when considering the waves' dynamics. However, the envelope over which Fr is allowed to oscillate (outlined in green) is consistent with a transcritical flow generation mechanism, because it includes considerable periods of $Fr = O(1)$, at least over some stage of the tidal cycle. Note that different oceanographic and bathymetric effects may combine to tune the hydraulic state such that it encompasses the transcritical regime. However, other environmental conditions may come into play so that the hydraulic state may not reach the transcritical regime during a complete tidal cycle, possibly explaining some SAR images in which no evidence of ISWs was found.

Finally, we recall that this analysis does not include the effects of changing either the stratification or the depth associated with the ISWs. On the one hand, stratification shows large intramonthly variability in the study region, which could render propagation speeds too extreme

to support ISW propagation (see colored profiles and corresponding phase speeds in Figure 5b). Results would, however, yield similar conclusions if stratification conditions were changed moderately. On the other hand, Figure 3 points to bottom bathymetry as an essential part of the ISW generation process. Interestingly, representative high-resolution bathymetric surveys (see Figure 1a for location) confirm these steep slopes for the area imaged in Figure 3a, as well as farther southeast along the shelf. An undulating seafloor was mapped at between approximately 60 m and 90 m depth, for which Froude numbers would still yield a plausible transcritical regime. Outside the waves' propagation areas, however, slopes appear much smoother and lacking forcing bathymetry (data available at http://maps.ngdc.noaa.gov/viewers/geophysics).

SUMMARY AND CONCLUSIONS

An extended SAR data set presented here provides an unprecedented view into ISW propagation along the Amazon continental shelf. Three different groups of ISWs were identified based on their sea surface signatures and main directions of propagation. While cross-shelf propagation has been confirmed (as documented in Jackson, 2004), the majority of the observations are consistent with upstream-propagating waves along the shelf, approximately in the opposite direction from the NBC (see Figure 1).

The ISW's two-dimensional horizontal structure is characterized based on the SAR imagery, including crest lengths and interpacket separations, which also revealed the waves to be present throughout the entire semidiurnal and fortnightly tidal cycles. Together with the available in situ data, the SAR images permitted a Froude number analysis, yielding hydraulic states frequently "drifting" in and out of a transcritical regime (see Figure 5). This result supports the majority of observed ISWs, whose SAR wavelengths are strongly related to shallow seafloor topography rather than to

typical semidiurnal tidal scales (see Figures 3 and 4). The present study provides convincing evidence of transcritical flow along the shelf and is consistent with theories of internal wave resonant generation, in which the NBC (modulated by the tides) flows over shallow seafloor topography and is likely to generate upstream-propagating waves.

While the lifespan of the ISWs remains an open question, SAR images reveal a wavefield extending more than 500 km across the Amazon River mouth. This large distance, together with their frequent occurrence, make ISWs potentially important in local dynamics between fresh riverine and open-ocean waters. Note that over shallow irregular seafloor, considerable dissipation and extra mixing might be expected due to strong sheared flow. Therefore, further research is warranted to understand the full extent of these observations, including hydrographic surveys and numerical modeling. ⦿

REFERENCES
Alford, M.H., T. Peacock, J.A. MacKinnon, J.D. Nash, M.C. Buijsman, L.R. Centuroni, S.-Y. Chao, M.-H. Chang, D.M. Farmer, O.B. Fringer, and others. 2015. The formation and fate of internal waves in the South China Sea. *Nature* 5(21):65–69, https://doi.org/10.1038/nature14399.

Almeida-Filho, R., F.P. Miranda, J.A. Lorenzzetti, E.C. Pedroso, C.H. Beisl, L. Landau, M.C. Baptista, and E.G. Camargo. 2005. RADARSAT-1 images in support of petroleum exploration: The offshore Amazon River mouth example. *Canadian Journal of Remote Sensing* 31:289–303, https://doi.org/10.5589/m05-013.

Alpers, W. 1985. Theory of radar imaging of internal waves. *Nature* 314:245–247, https://doi.org/10.1038/314245a0.

Alpers, W., and I. Hennings. 1984. A theory of the imaging mechanism of underwater bottom topography by real and synthetic aperture radar. *Journal of Geophysical Research* 89:10,529–10,546, https://doi.org/10.1029/JC089iC06p10529.

Beardsley, R.C., J. Candela, R. Limeburner, W.R. Geyer, S.J. Lentz, B.M. Castro, D. Cacchione, and N. Carneiro. 1995. The M_2 tide on the Amazon shelf. *Journal of Geophysical Research* 100(C2):2,283–2,319, https://doi.org/10.1029/94JC01688.

Bogucki, D., T. Dickey, and L.G. Redekopp. 1997. Sediment resuspension and mixing by resonantly generated internal solitary waves. *Journal of Physical Oceanography* 27:1,181–1,196, https://doi.org/10.1175/1520-0485(1997)027<1181:SRAMBR>2.0.CO;2.

Brandt, P., A. Rubino, and J. Fisher. 2002. Large-amplitude internal solitary waves in the North Equatorial Countercurrent. *Journal of Physical Oceanography* 32:1,567–1,573, https://doi.org/10.1175/1520-0485(2002)032<1567:LAISWI>2.0.CO;2.

Castro, B.M., and L.B. Miranda 1998. Physical oceanography of the western Atlantic continental shelf located between 4°N and 34°S. Pp. 209–251 in *The Sea, Volume 11: The Global Coastal Ocean: Regional Studies and Syntheses.* A.R. Robinson and K.H. Brink, eds, John Wiley and Sons, New York.

Coe, M.T., M.H. Costa, A. Botta, and C.M. Birkett. 2002. Long-term simulations of discharge and floods in the Amazon basin. *Journal of Geophysical Research* 107(D20), https://doi.org/10.1029/2001JD000740.

Coles, V.J., M.T. Brooks, J. Hopkins, M.R. Stukel, P.L. Yager, and R.R. Hood. 2013. The pathways and properties of the Amazon River Plume in the tropical North Atlantic Ocean. *Journal of Geophysical Research* 118:6,894–6,913, https://doi.org/10.1002/2013JC008981.

Cummins, P.F., S. Vagle, L. Armi, and D.M. Farmer. 2003. Stratified flow over topography: Upstream influence and generation of nonlinear internal waves. *Proceedings of the Royal Society of London A* 459:1,467–1,487, https://doi.org/10.1098/rspa.2002.1077.

da Silva, J.C.B, M.C. Buijsman, and J.M. Magalhaes. 2015. Internal waves on the upstream side of a large sill of the Mascarene Ridge: A comprehensive view of their generation mechanisms and evolution. *Deep Sea Research Part I* 99:87–104, https://doi.org/10.1016/j.dsr.2015.01.002.

da Silva, J.C.B., S.A. Ermakov, I.S. Robinson, D.R.G. Jeans, and S.V. Kijashko. 1998. Role of surface films in ERS-SAR signatures of internal waves on the shelf: Part 1. Short-period internal waves. *Journal of Geophysical Research* 103:8,009–8,031, https://doi.org/10.1029/97JC02725.

Egbert, G.D., and S.Y. Erofeeva. 2002. Efficient inverse modeling of barotropic ocean tides. *Journal of Oceanic and Atmospheric Technology* 19:183–204, https://doi.org/10.1175/1520-0426(2002)019<0183:EIMOBO>2.0.CO;2.

Farmer, D.M., and L. Armi. 1999. The generation and trapping of internal solitary waves over topography. *Science* 283:188–190, https://doi.org/10.1126/science.283.5399.188.

Geyer, W.R., R.C. Beardsley, S.J. Lentz, J. Candela, R. Limeburner, W.E. Johns, B.M. Castro, and I.D. Soares. 1996. Physical oceanography of the Amazon Shelf. *Continental Shelf Research* 16(5–6):575–616, https://doi.org/10.1016/0278-4343(95)00051-8.

Hübscher, C., A. Figueiredo, L. Kruse, and V. Spieß. 2002. High-resolution analysis of the deposition pattern on the Amazon sub-aquatic delta and outer continental shelf. *Marine Geophysical Researches* 23:(3):209–222, https://doi.org/10.1023/A:1023603221876.

Inall, M.E., G.I. Shapiro, and T.J. Sherwin. 2001. Mass transport by non-linear internal waves on the Malin Shelf. *Continental Shelf Research* 21(13–14):1,449–1,472, https://doi.org/10.1016/S0278-4343(01)00020-6.

Ivanov, V.A., L.I. Ivanov, and A.D. Lisichenok. 1990. Redistribution of energy of the internal tidal wave in the North Equatorial Countercurrent region. *Soviet Journal of Physical Oceanography* 1:383–386, https://doi.org/10.1007/BF02196837.

Jackson, C.R. 2004. *An Atlas of Internal Solitary-like Waves and their Properties*, 2nd ed. Global Ocean Associates, Alexandria, VA, 560 pp., http://www.internalwaveatlas.com.

Jackson, C.R. 2007. Internal wave detection using the Moderate Resolution Imaging Spectroradiometer (MODIS). *Journal of Geophysical Research* 112, C11012, https://doi.org/10.1029/2007JC004220.

Jackson, C.R., J.C.B. da Silva, and G. Jeans. 2012. The generation of nonlinear internal waves. *Oceanography* 25(2):108–123, https://doi.org/10.5670/oceanog.2012.46.

Johns, W.E., T.N. Lee, R.C. Beardsley, J. Candela, R. Limeburner, and B. Castro. 1998. Annual cycle and variability of the North Brazil Current. *Journal of Physical Oceanography* 28:103–128, https://doi.org/10.1175/1520-0485(1998)028<0103:ACAVOT>2.0.CO;2.

Klymak, J.M., S. Legg, M.H. Alford, M. Buijsman, R. Pinkel, and J.D. Nash. 2012. The direct breaking of internal waves at steep topography. *Oceanography* 25(2):150–159, https://doi.org/10.5670/oceanog.2012.50.

Lamb, K.G. 2014. Internal wave breaking and dissipation mechanisms on the continental slope/shelf. *Annual Review of Fluid Mechanics* 46:231–254, https://doi.org/10.1146/annurev-fluid-011212-140701.

Lentz, S.J. 1995. Seasonal variations in the horizontal structure of the Amazon plume inferred from historical hydrographic data. *Journal of Geophysical Research* 100:2,391–2,400, https://doi.org/10.1029/94JC01847.

Lodge, D.W.S. 1983. Surface expression of bathymetry on Seasat synthetic aperture radar images. *International Journal of Remote Sensing* 4:639–653, https://doi.org/10.1080/01431168308948580.

Lorenzzetti, J.A., and F.G. Dias. 2013. Internal solitary waves in the Brazilian SE continental shelf: Observations by synthetic aperture radar. *International Journal of Oceanography* 2013:403259, https://doi.org/10.1155/2013/403259.

Magalhaes, J.M., J.C.B. da Silva, M.C. Buijsman, and C.A.E. Garcia. 2016. Effect of the North Equatorial Counter Current on the generation and propagation of internal solitary waves off the Amazon shelf (SAR observations). *Ocean Science* 12:243–255, https://doi.org/10.5194/os-12-243-2016.

Melville, W.K., and K.R. Helfrich. 1987. Transcritical two-layer flow over topography. *Journal of Fluid Mechanics* 178:31–52, https://doi.org/10.1017/S0022112087001101.

Moura, R.L., G.M. Amado-Filho, F.C. Moraes, P.S. Brasileiro, P.S. Salomon, M.M. Mahiques, A.C. Bastos, M.G. Almeida, J.M. Silva, B.F. Araujo, and others. 2016. An extensive reef system at the Amazon River mouth. *Science Advances* 2(4):e1501252, https://doi.org/10.1126/sciadv.1501252.

Moum, J.N., D.M. Farmer, W.D. Smyth, L. Armi, and S. Vagle. 2003. Structure and generation of turbulence at interfaces strained by internal solitary waves propagating shoreward over the continental shelf. *Journal of Physical Oceanography* 33:2,093–2,112, https://doi.org/10.1175/1520-0485(2003)033<2093:SAGOTA>2.0.CO;2.

Muller-Karger, F.E., C.R. McClain, and P.L. Richardson. 1988. The dispersal of the Amazon's water. *Nature* 333:56–59, https://doi.org/10.1038/333056a0.

Nikiema, O., J-L. Devenona, and M. Bakloutib. 2007. Numerical modeling of the Amazon River plume. *Continental Shelf Research* 27:873–899, https://doi.org/10.1016/j.csr.2006.12.004.

Quaresma, L.S., J. Vitorino, A. Oliveira, and J.C.B. da Silva. 2007. Evidence of sediment resuspension by nonlinear internal waves on the western Portuguese mid-shelf. *Marine Geology* 246:123–143, https://doi.org/10.1016/j.margeo.2007.04.019.

Shroyer, E.L., J.N. Moum, and J.D. Nash. 2010. Vertical heat flux and lateral mass transport in nonlinear internal waves. *Geophysical Research Letters* 37, L08601, https://doi.org/10.1029/2010GL042715.

Shuchman, R.A., D.R. Lyzenga, and G.A. Meadows. 1985. Synthetic aperture radar imaging of ocean-bottom topography via tidal-current interactions: Theory and observations. *International Journal of Remote Sensing* 6:1,179–1,200, https://doi.org/10.1080/01431168508948271.

Smyth, W.D., J.N. Moum, and J.D. Nash. 2011. Narrowband oscillations in the upper equatorial ocean: Part II. Properties of shear instabilities. *Journal of Physical Oceanography* 41(3):412–428, https://doi.org/10.1175/2010JPO4451.1.

Thompson, D.R., and R.F. Gasparovic. 1986. Intensity modulation in SAR images of internal waves. *Nature* 320:345–348, https://doi.org/10.1038/320345a0.

AUTHORS
Carlos A.D. Lentini is Associate Professor, Department of Earth and Environmental Physics, Physics Institute, Federal University of Bahia, Salvador, BA, Brazil. **Jorge M. Magalhães** is a post-doctoral researcher and **José C.B. da Silva** (jdasilva@fc.up.pt) is Associate Professor in the Department of Geosciences, Environment, and Spatial Planning, and Interdisciplinary Centre of Marine and Environmental Research, University of Porto, Porto, Portugal. **João A. Lorenzzetti** is Senior Researcher, Remote Sensing Division, National Institute for Space Research, São José dos Campos, SP, Brazil.